Mechanical properties of poly(ethylene terephthalate) at the near surface from depth sensing experiments

By A. Flores and F. J. Baltá Calleja

Instituto de Estructura de la Materia, CSIC, Serrano 119, 28006 Madrid, Spain

ABSTRACT

The viscoelastic-plastic properties of glassy PET in the micron and submicron range have been investigated by means of load-displacement analysis from depth sensing experiments. Experimental data have been modelled using two methods: a) assuming the elastic behaviour during initial unloading as that of a cylindrical punch, b) using a power law relation. The creep behaviour under the indenter has been examined. Furthermore, the influence of the maximum penetration depth and loading and holding times on the hardness values is discussed. Hardness data from the depth sensing and imaging methods are shown to be in good agreement. When using the depth sensing method, hardness values are shown to be constant with decreasing penetration depth ($0.5\mu m \leq h_{max} \leq 9\mu m$), provided a correction procedure to account for the indenter tip defect is applied. The Young's modulus derived from the compliance method has been studied and results are discussed in the light of the various testing conditions employed.

§ 1. INTRODUCTION

The indentation test is one of the simplest ways to measure the mechanical properties of a material. The micromechanical behaviour of polymers and the correlation with morphology and microstructure have been widely investigated over the past two decades (Baltá Calleja 1985, 1994; Baltá Calleja and Fakirov 1997). Conventional microindentation instruments are based on the optical measurement of the residual impression produced by a sharp indenter penetrating the specimen surface under a given load at a known rate. Microhardness is obtained by dividing the peak load by the contact area of impression. It has been shown that post-indentation microhardness of plastic polymers is a good measure of microhardness at peak load due to a negligible recovery of the area of impression (Eyerer and Lang 1972). While hardness, defined in this way, is an indicator of the irreversible plastic deformation processes, information about the elastic recovery of the indentation penetration depth is mostly lost. On a microindentation experiment, typical loads range from 10^2-10^3 mN. When these loads are applied onto the surface of hard semicrystalline polymers such as poly(ethylene terephthalate) (PET), the penetration depths range between 4–10 μm (Santa Cruz *et al.* 1991).

The need to mechanically characterize the surface of very thin films and near surfaces has led to the development of ultramicro and nanoindentation testers (Loubet *et al.* 1984; Doerner and Nix 1986; Oliver and Pharr 1992; Pharr *et al.* 1992; Raman and Berriche 1992; Blau *et al.* 1993; Vancoille *et al.* 1993; Kulkarni and Bhushan 1996, Briscoe *et al.* 1996). Continuous load-displacement monitoring, as the indenter is driven into and withdrawn from the film, substitutes the imaging method used in conventional microindenters. Smaller loads can be applied leading to penetration depths within the

sub-micron scale. The compliance method opens up the possibility of investigating the mechanical properties of a material at the near surface. In addition, the elastic recovery of the indentation upon the removal of the load can be investigated.

Indentation testing in the sub-micron scale has been widely explored in metals and ceramics (Loubet *et al.* 1984, Doerner and Nix 1986, Oliver and Pharr 1992, Pharr *et al.* 1992, Raman and Berriche 1992, Blau *et al.* 1993, Vancoille *et al.* 1993, Kulkarni and Bhushan 1996). However, there is still little research on the viscoelastic-plastic properties of polymers derived from depth sensing experiments. This is probably due to the time-dependent mechanical behaviour which complicates the interpretation of the results. Hardness and elastic modulus values of poly(isobutadiene) rubber, poly(ether-ether ketone), poly(methyl methacrylate) (PMMA) and nylon-6 have been reported (Briscoe *et al.* 1996). In all cases, the indentation depth lay within the micron regime ($\geq 2\mu m$). In a recent paper (Briscoe and Sebastian 1996), the influence of the indenter geometry on the hardness and Young's modulus values of PMMA has been carefully examined. These authors show, in addition, that the values of hardness measured directly from the residual image, correlate well with those computed using the compliance method. The plastic, elastic and flow properties of amorphous and uniaxially drawn PET containing different fillers have also been reported (Ion *et al.* 1990). The penetration depths of the impressions produced ranged between 0.5-5 μm. In the micron regime, hardness values reported were about a factor two greater than H of an amorphous PET sample measured using the imaging technique (Baltá Calleja *et al.* 1993). The discrepancy is possibly due to the presence of fillers in the sample investigated by means of the depth sensing technique although the authors of the former paper advised not to rely upon the absolute values of hardness.

The aims of the present paper are the following: a) to discuss the difference in hardness/elastic modulus values of amorphous PET, obtained from a depth sensing experiment, according to which theoretical assumptions are used; b) to compare H results from the compliance and the imaging methods in a wide range of experimental conditions; c) to examine the influence of the test parameters (loading time and holding time) on the mechanical properties obtained; d) to investigate the plastic properties of PET in the sub-micron range and compare to the H values obtained in the micron regime.

§ 2. EXPERIMENTAL

2.1. *Materials and sample mounting*

Amorphous PET supplied by Kalle (Germany) in the form of a 200 μm thick film was investigated. It is known that ageing affects the hardness values of amorphous PET during the first hours of storage (Ania *et al.* 1989). In order to avoid ageing effects during the performance of our experiments, a sample stored for three years at room temperature has been chosen. For the compliance method, the specimen was glued onto a metal holder to avoid air gaps between the sample and the test piece stage. The sample was then positioned on the test stage of the ultramicroindenter and tightened with the help of band fasteners. The same PET sample was used to measure hardness values by means of the imaging method.

2.2. *Imaging method: microhardness measurements*

A Leitz microindenter was used to measure hardness at room temperature. The indenter is a Vickers square-based diamond pyramid with included angles φ=136° between non-adjacent faces. The force applied was 249 mN. The time at which this force was held varied between 6 and 1000 seconds. For a holding time of 6 seconds, a load of

147 mN was also used. Hardness was measured from the residual projection of the area of indentation according to (Tabor 1951):

$$H = \frac{P}{A} \tag{1}$$

where A is the projected area of the indentation. A is related to the diagonal of the residual impression, d, through:

$$A = 24.5\left(\frac{d}{7}\right)^2 \tag{2}$$

Using equation (2), we may write equation (1) as:

$$H = 2\frac{P}{d^2} \tag{3}$$

The length of the impression was measured to ±0.5μm with a microscope equipped with a filar eyepiece.

2.3. *Compliance method: ultramicroindentation experiments*

Depth sensing experiments were carried out in a Shimadzu dynamic ultramicroindentation tester. In this system, the indenter enters the test surface vertically. The load is applied through a load generator which comprises a fixed permanent magnet and movable force coil. When electric current flows through the coil, the electromagnetic force is generated in proportion to the coil current. The coil is controlled to obtain the desired load. The electromagnetic force generated is transmitted to the indenter via a lever and an indenter supporting shaft. Indentation depth is measured by using a differential transformer positioned near the indenter. The minimum load that can be applied with this instrument is 0.1 mN with an accuracy of ±1%. The displacement of the indenter is recorded with an accuracy of 10^{-3} μm. In order to better compare the measurements of this technique with those of the imaging method, a Vickers diamond

pyramid was used to make indentations. Figure 1 shows a typical load-displacement curve for one of the PET samples investigated in this paper. On loading, the force was incremented at constant velocity. In the compliance curve of figure 1, the rate at which the force is incremented is of 6.6 mN/s. The depth represents the contribution of, both, the elastic and plastic displacements. The loading curve was followed by a period of time, Δt_{hold}, at which the peak load is held constant. The value of Δt_{hold} in figure 1 corresponds to 200 seconds. During unloading, the load is always reduced at the same rate as in the loading cycle. In this case, the elastic displacements are recovered.

Three sets of experiments were carried out in order to independently study the influence of the three main parameters (holding time, loading rate and maximum load) on the viscoelastic-plastic properties of the polymer. The experimental parameters values used are collected in table 1.

In the first set of experiments, a maximum load, P_{max}, of 147 mN (in the range of the loads used in the imaging technique) was reached at a loading rate, $\dot{P}$, of 13.2 mN/s and held thereafter for a period of time which varied between 6 and 10^3 seconds.

In a second set of experiments, the loading rate was varied between 0.47 and 13.2 mN/s to reach again a maximum 147 mN peak load which was held for 6 and 200 seconds.

For the comparative study of the plastic properties of PET in the micron and sub-micron regime (third set of experiments), the maximum load was varied between 0.98 and 245 mN. The loading rate was adjusted on each experiment to maintain the time employed in the loading cycle, t_{load}, between 7-14 seconds. Δt_{hold} was 6 seconds in all cases.

§ 3. ANALYSIS OF THE COMPLIANCE CURVES

3.1. *Derivation of mechanical properties*

Values of hardness and elastic modulus were obtained following the procedure of Doerner and Nix (1986) and Oliver and Pharr (1992). Both procedures use the slope of the unloading curves as a measure of the elastic properties of the sample.

Doerner and Nix modelled the elastic behaviour of the indentation during the initial unloading as that of a blunt punch. These authors used Sneddon's analysis of the indentation of an elastic half space by a flat cylindrical punch (Sneddon 1965). The elastic modulus, E, was derived from the initial unloading slope following:

$$E_r = \sqrt{\frac{\pi}{A}}\frac{S}{2} \tag{4}$$

$$\text{where } \frac{1}{E_r} = \frac{1-\nu^2}{E} + \frac{1-\nu_o^2}{E_o} \tag{5}$$

and where $S=\Delta P/\Delta h$ is the initial unloading stiffness, A the projected area of contact, E_r the reduced modulus, E and ν Young's modulus and Poisson's ratio of the material respectively and E_o and ν_o Young's modulus and Poisson's ratio of the indenter respectively. $\Delta P/\Delta h$ is evaluated by fitting a tangent to the initial portion of the unloading curve. For a perfect Vickers geometry, $A = 24.5\, h_p^2$, where h_p (plastic depth) is the depth of the indenter in contact with the sample at maximum load. Doerner and Nix suggest to estimate the plastic depth by extrapolating to zero load the tangent fitted to the initial portion of the unloading curve (see figure 1). In the present study, we have used 20% of the upper part of the unloading curve to derive $\Delta P/\Delta h$. The reduced elastic modulus, E_r, is introduced to account for the displacement contribution of a non-rigid indenter. For

diamond, $\nu_o = 0.07$ and $E_o = 1141$ GPa (Simmons and Wang 1971). Poisson's ratio for PET is taken to be 0.5 (Birley *et al.* 1992). The elastic modulus of PET is around 2.5 GPa (see below). Then, $(1-\nu_o^2)/E_o$ is negligible in equation (5) and equation (4) leads to:

$$E=\sqrt{\frac{\pi}{A}}\frac{S}{2}(1-\nu^2) \tag{6}$$

Hardness is derived through:

$$H=\frac{P_{max}}{A} \tag{7}$$

where P_{max} is the maximum load applied.

Pharr et al. showed that equation (4) holds for all indenters than can be considered as bodies of revolution (Pharr *et al.* 1992). Moreover, they indicated that it is possible to use eq. (4) for a Vickers geometry without great error (1.2% error in the unloading stiffness values). Oliver and Pharr simultaneously developed a method to evaluate the initial unloading stiffness, S, and the contact penetration depth at peak load, h_c, for several indenter geometries (Oliver and Pharr 1992). Once S and h_c are determined, E and H are evaluated through equations (6) and (7) respectively, where $A=24.5\ h_c^2$ for a perfect Vickers geometry. The new method of analysis uses a power law relation to describe the unloading curves:

$$P = \alpha(h - h_f)^m \tag{8}$$

where P is the load, $h-h_f$ the elastic displacement (see figure 1) and α and m are material constants. We have used a least square fitting procedure to fit the entire experimental unloading data to a power law curve. In this way, the parameters α, m, and h_f are determined. The initial unloading stiffness, $S=(\partial P/\partial h)_{max}$, is found by analytically differentiating expression (8) and evaluating the derivative at the peak load and displacement. Oliver and Pharr calculated the contact depth, h_c, following:

$$h_c = h_p + (1-\epsilon)\,(h_{max}-h_p) \qquad (9)$$

where h_p represents the intercept of the initial unloading slope with the displacement axis (as shown in figure 1), h_{max} is the maximum displacement reached by the indenter (see figure 1) and ϵ is a geometric constant. The ϵ value depends on which of the indenter geometries best describes the experimental data (see Oliver and Pharr 1992 for more details). In our case, an ϵ value of 0.72 was chosen, which corresponds to a conical geometry. Note that $\epsilon = 0.72$ implies that h_c is always higher than h_p.

3.2. *Sources of error*

To minimize the error on the determination of the true zero of indentation depth, the experimental loading curve was fitted to a power law function of the type (Briscoe and Sebastian 1996):

$$P = m(h-h_o)^n \qquad (10)$$

where m is a material constant, n is the index of the deformation and h_o is the true zero point.

To correct for the instrument compliance, C_f, the compliance data, $C = S^{-1}$, were plotted versus $1/\sqrt{A}$ for the biggest indentation sizes (load ranges from 9.8 to 245 mN). A is that of an ideal Vickers indenter. The y-axis intercept was used as a first estimate of the frame compliance, being:

$$C_f = \frac{1}{S} - \frac{1}{\sqrt{A}}\frac{\sqrt{\pi}}{2E}(1-\nu^2) \qquad (11)$$

The method assumes an E value which is independent of the indentation depth. The first estimate of the frame compliance was used to correct the experimental compliance curves, and new values of A were derived. The procedure was iterated several times until

convergence was achieved. The machine compliance correction is more important for materials with high elastic modulus and low hardness. In our case, the machine compliance was negligible except for the E value corresponding to 245 mN peak load, where a 7% increase in E was obtained.

§ 4. RESULTS AND DISCUSSION

4.1. *Plastic properties*

Holding and loading time dependence

The derivation of hardness from load-displacement data requires an evaluation of the elastic displacements during the indentation recovery. Time-dependent plastic effects contributing to the initial portion of the unloading curve lead to an unsatisfactory analysis (Turnbull and White 1996). To discard the time-dependent displacements during unloading, one common procedure is to hold the maximum load for a sufficiently long period of time. However, microindentation experiments on polymeric materials had shown that hardness is strongly dependent on the time of application under the peak load (Baltá Calleja 1985). Usually, hardness values derived from microindentation experiments are referred to short holding times (a few seconds) so as to minimize the creep of the sample under the indenter (Baltá Calleja 1985). In depth sensing instruments, increasing the holding time at peak load diminishes the plastic effects masking the elastic displacements but on the other side, hardness values are modulated by the creep effect. The need to reach a compromise to select an appropriate value of the holding time, prompted us to investigate the hardness variation with Δt_{hold}.

Figure 2 shows the double logarithmic plot of H derived from the compliance method, H_{compl}, vs. holding time (peak load=147mN, loading rate=13.2mN/s). The

cylindrical punch approximation and the power law fitting method were used in the data analysis. Hardness values obtained from the imaging method, H_{imag}, are included in figure 2 for comparison. From microindentation experiments on a wide range of polymers, the time dependent part of the plastic deformation is shown to follow a function of the type (Baltá Calleja 1985):

$$H = H_o t^{-k}$$

where H_o is the hardness measured at t=1 min and k is the creep constant. It is interesting to observe the same type of creep effect in, both, depth sensing and imaging experiments. Hardness values do not seem to be sensitive to time-dependent plastic contributions to the unloading as no significant deviation from the creep curves at the shortest times is observed. In the following, a holding time of six seconds will be employed to evaluate H. This arbitrary criterion arises from the fact that H_{imag} is frequently measured using a holding time of six seconds (Baltá Calleja 1985). Therefore, if we wish to compare H_{compl} with H_{imag}, it seems reasonable to use the same holding time at maximum load in both experiments. Other authors have also used a holding time of a few seconds on their microhardness testing using the compliance method (see Doerner and Nix 1986, where Δt_{hold}=10s). Figure 2 shows that H_{compl} analysed using the power-law fitting method is very close to H_{imag}, the differences lying within the error limits. This result suggests that, at least for amorphous PET, post-indentation hardness as measured using the imaging technique is a good measure of hardness under load. On the other hand, H_{compl} values derived from the cylindrical punch method and using h_p as the contact depth, are 10-15% higher than H_{imag}. This difference could be due to: i) an inaccurate determination of the initial unloading stiffness when using the cylindrical punch method. S is known to depend on how many data are used in the linear fit to the upper part of the

unloading (Oliver and Pharr 1992); ii) an underestimation of the contact depth, h_p, which is directly derived from the intercept of the unloading slope at zero load. To elucidate which one of the two possibilities is responsible for the high H_{compl} values obtained using Doerner and Nix's analysis, figure 2 includes hardness values obtained when fitting a tangent to 1/5 of the upper part of the unloading (cylindrical punch approximation) and calculating the contact depth using eq. (9). These hardness values are represented by squares. It is clear that H data as calculated using the power law fitting method and H values from the cylindrical punch approximation are very close to each other, the difference lies within the error limits, when the criterion adopted to calculate the contact depth is the same. However, if the stiffness were calculated by the cylindrical punch method using a larger fraction of the unloading curve, deviations in the H values with respect to those obtained using the power law method would be expected (Oliver and Pharr 1992).

Figure 3 shows the plot of the hardness value as a function of the loading time (peak load=147mN, holding time=6s). No considerable H variation with t_{load} is obtained.

Penetration depth influence on hardness

Figure 4a illustrates the variation of H as a function of the maximum penetration depth reached by the indenter when applying different peak loads (loading time=7-14s, holding time=6s). Hardness is shown to be independent of the indentation depth when this is larger than 2 μm. In this range, H_{compl} obtained when the contact depth is determined using equation (9), is comparable to H_{imag}. At h_{max}<1μm, there is a pronounced H increase with decreasing penetration depth. There are two possible reasons for the H increase when h_{max} is below 1 μm: i) an intrinsic higher H value at the

near surface or ii) a change in the contact area to depth relation, $A(h_c)$, due to a non-negligible tip defect at these penetration depths. A harder outer skin of ~ 20 μm has been observed in semicrystalline poly(ethylene naphthalene-2,6-dicarboxylate) (PEN) which was annealed above the glass transition temperature (Rueda *et al.* 1994). This hardening effect of the outer layer could be explained due to a thermal gradient during the annealing experiment which could give rise to a higher crystallinity at the surface. Although this is not the case in amorphous PET, the first 30 μm of the sample were removed to check the hardness values below the surface. No significant differences in hardness were found. Thus, the use of $A(h_c)$ as the area of a perfect pyramid geometry is not anymore valid for penetration depths smaller than 1 μm. Several methods have been developed to account for the difference between the genuine contact area and the area corresponding to an ideally sharp indenter (Mencík and Swain 1995). We have used a procedure which assumes that for an ideally sharp indenter, the load is proportional to the square of the depth of indenter penetration. That is to say, that the n exponent in equation (10) takes a value of 2. This is, indeed, the n-value obtained when fitting our experimental loading curves for the largest indentations ($h_{max} \geq 2\mu m$) to a power law function. The h_o value in equation (10) corrects for the experimental uncertainty in the location of the point of initial contact and the magnitude of the tip defect. The latter causes that the experimental loading curves depart from $P \sim (h-h_o)^2$ at small penetration depths. At these penetration depths, the difference between the observed and the ideal penetration depth values provides the correction which should be introduced in the measured penetration depth of the compliance curves corresponding to indentations of small size. The real contact area can now be calculated as $A=24.5\ h'^2_c$ (or analogously: $A=24.5\ h'^2_p$) where h'_c (or h'_p) represents the corrected contact depth value. Figure 4b

shows the H values as a function of the maximum penetration depth when the above mentioned correction procedure, which accounts for the indenter tip defect, is applied. From these results, we can conclude that hardness of glassy PET remains constant with decreasing penetration depth, within the range of penetration depths investigated.

4.2. *Elastic properties*

Holding time dependence

Figure 5 shows the variation of Young's modulus versus holding time at peak load (P_{max}=147mN; $\dot{P}$=13.2mN/s). E derived from the cylindrical punch approximation using either h_p or h_c, appears to be constant over the holding times considered. On the contrary, E derived from the power-law fitting method shows a tendency to increase with Δt_{hold} showing a higher rate in the range $0.1 < \Delta t_{hold} < 3$ minutes. To clarify this finding, the variation of $\Delta P/\Delta h$ and $(\partial P/\partial h)_{max}$ vs. holding time has been represented in figure 6. This variation directly supports the results in figure 5. The steep increase of $(\partial P/\partial h)_{max}$ cannot be explained in terms of the time-dependent plastic contribution to the initial elastic recovery of the indentation. Such an effect would produce a $(\partial P/\partial h)_{max}$ decrease with increasing holding time. A careful examination of the load-displacement curves at different holding times shows a similar rate of depth recovery at the initial stages of unloading (see figure 7). However, at approximately 1/4 of the unloading curve, the withdrawal of the indenter is slower at the highest Δt_{hold}. The cylindrical punch method makes use of the initial part of unloading. Thus, $\Delta P/\Delta h$ only shows a slight variation with Δt_{hold}. On the other hand, the power law fitting method employs all the force-displacement data during the indentation recovery. In this case, $(\partial P/\partial h)_{max}$ markedly varies with Δt_{hold} . This result suggests than an appreciably time-dependent

elastic recovery is present in the unloading curves. The viscoelastic response of the material seems to vary with the holding time at maximum load in a way that the shorter Δt_{hold} is, the higher is the viscoelastic recovery during unloading. The fact that E values (power law fitting) do not seem to level-off at the highest Δt_{hold} , seems to suggest that, at this holding time, there is still some retarded elastic recovery present during unloading.

Loading time dependence

Figure 8a and b illustrates the variation of E as a function of the time required in the loading cycle for Δt_{hold} of 6 and 200 seconds respectively (P_{max}=147mN). For a Δt_{hold} of 6 seconds, Young's modulus values show a steep increase at Δt_{hold} < 1 min and a further increase up to t_{load} ~ 5 min. In figure 8b, where Δt_{hold} = 200 s, E shows an appreciably increase up to ~ t_{load} =1min where a level-off in the E values is observed. To understand the results obtained in figures 8a and b, force-displacement curves corresponding to t_{load} =11 s and 311 s at different Δt_{hold} have been represented in figure 9. Figure 9a shows the compliance curves for a loading rate $\dot{P}$=0.47 mN/s (t_{load} =311 s) and 13.2 mN/s (t_{load}=11s), both with a holding time of 6 seconds. At the lowest loading rate, the depth registered during the holding time is much smaller than that corresponding to the highest loading rate. This effect could be explained in terms of inertial plastic effects at the highest loading rate. When the indenter is withdrawn, an abnormal shape in the upper part of the unloading is observed at the lowest $\dot{P}$. This curvature could be explained in terms of the sample creep under the indenter. At the same time, a quick look to the entire shape of the unloading curve reveals that the withdrawal of the indenter is slower at the slowest loading rate, suggesting a different viscoelastic response during unloading at different t_{load}. It seems that viscoelastic

recovery during unloading is minimized at the lowest $\dot{P}$. The fact that a creep effect is not observed during the initial stages of unloading for $\dot{P}$=13.2 mN/s, could be possibly due to the influence of the viscoelastic recovery of the indentation masking the creep effect. From figure 9a it is obvious that the initial unloading stiffness increases with decreasing loading rate (or increasing t_{load}), leading to the E increase with increasing t_{load} observed in figure 8a. Figure 9b shows the load-displacement data corresponding to $\dot{P}$=0.47 and 13.2 mN/s. The holding time at maximum load is 200s. The first observation is that the creep effect present in the upper part of the unloading when t_{load}=311s, Δt_{hold}=6s, is missing when the holding time is increased up to 200 sec. This fact facilitates the calculation of the initial unloading stiffness leading to more reliable values. The shape of the unloading curve is still different for the highest and lowest t_{load}. At the largest t_{load}, the viscoelastic recovery during unloading seems to be minimized. S does not substantially vary for t_{load}>1min leading to E values independent of t_{load}. Figure 8b shows that two different E values at high t_{load} are obtained for the cylindrical punch approximation and the power law method when both procedures use equation (9) to calculate the contact depth. This finding arises from the different S values estimated. As previously mentioned, the stiffnesses values estimated using the cylindrical punch method are sensitive to the fraction of the unloading curve used. Thus, the S values derived using this last method seem to be underestimated leading to slightly smaller values of E with respect to the power law method.

In summary, to obtain reliable values of the Young's modulus, the experimental conditions have to be chosen appropriately. Our results show that decreasing the loading rate and increasing the holding time at maximum load gives satisfactory and consistent E values.

§ 5. CONCLUSIONS

From the results obtained we may draw the following conclusions:

(1) The H data obtained using the power law method and H values from the cylindrical punch approximation (for the portion of unloading curve used) agree with each other within the error limits when the criterion used to calculate the contact depth is the same.

(2) The H data from the compliance and from the imaging methods appear to be in agreement with each other in the range of holding times used.

(3) The creep behaviour under the indenter derived from the compliance method yields a H decrease with time: $H \sim t^{-k}$, similar to that obtained by the imaging method.

(4) The H_{compl} values are shown to be independent on the loading time (t_{load}) for small holding times.

(5) Analysis of the H values versus penetration depth shows that for $h_{max} \geq 1$ μm, H_{compl} is constant while for $h_{max} < 1$ μm, H_{compl} exhibits an increase with decreasing penetration depth. This apparent change in hardness is due to a non-negligible tip defect at small depths of penetration. After correction for the indenter tip defect, H is shown to be constant over the range of penetration depths investigated.

(6) The power law method turns out to be more reliable than the cylindrical punch method for the evaluation of the elastic modulus values.

(7) For short loading times, E (power law method) increases with increasing Δt_{hold}. At short holding times, E is an increasing function of t_{load} while at long holding times, E tends to remain constant for $t_{load} > 1$ min.

ACKNOWLEDGEMENTS

Grateful acknowledgement is due to the Dirección General de Investigación Científica y Técnica (DGICYT), Spain, for support of this investigation (Grant PB94-0049).

REFERENCES

ANIA, F., MARTÍNEZ-SALAZAR, J., BALTÁ CALLEJA, F. J., 1989, *J. Mater. Sci.*, **24**, 2934.

BALTÁ CALLEJA, F. J., 1985, *Adv. Polym. Sci.*, **66**, 117.

BALTÁ CALLEJA, F. J., 1994, *Trends Polym. Sci.*, **2**, 419.

BALTÁ CALLEJA, F. J., FAKIROV, S., 1997, *Trends Polym. Sci.*, **5**, 246.

BALTÁ CALLEJA, F. J., SANTA CRUZ, C., ASANO, T., 1993, *J. Polym. Sci.: Part B: Polym. Phys.*, **31**, 557.

BIRLEY, A. W., HAWORTH, B., BATCHELOR, J., 1992, *Physics of Plastics* (New York: Oxford University Press).

BLAU, P. J., KEISER, J. R., JACKSON, R. L., 1993, *Mater. Charac.*, **30**, 287.

BRISCOE, B. J., SEBASTIAN, K. S., SINHA, S. K., 1996, *Phil. Mag. A*, **74**, 1159.

BRISCOE, B. J., SEBASTIAN, K. S., 1996, *Proc. R. Soc. Lond. A*, **452**, 439.

DOERNER, M. F., NIX, W. D., 1986, *J. Mater. Res.*, **1**, 601.

EYERER, P., LANG, G., 1972, *Kunststoffe*, **62**, 322.

ION, R. H., POLLOCK, H. M., ROQUES-CARMES, C., 1990, *J. Mater. Sci.*, **25**, 1444.

KULKARNI, A. V., BHUSHAN, B., 1996, *Thin Solid Films*, **291**, 206.

LOUBET, J. L., GEORGES, J. M., MARCHESINI, O., MEILLE, G., 1984, *J. Tribology*, **106**, 43.

MENCÍK, J., SWAIN, M.V., 1995, *J. Mater. Res.*, **10**, 1491.

OLIVER, W. C., PHARR, G. M., 1992, *J. Mater. Res.*, **7**, 1564.

PHARR, G. M., OLIVER, W. C., BROTZEN, F. R., 1992, *J. Mater. Res.*, **7**, 613.

RAMAN, V., BERRICHE, R., 1992, *J. Mater. Res.*, 7, 627.

RUEDA, D. R., VIKSNE, A., MALERS, L., BALTÁ CALLEJA, F. J., ZACHMANN, H. G., 1994, *Macromol. Chem. Phys.* **195**, 3869.

SANTA CRUZ, C., BALTÁ CALLEJA, F. J., ZACHMANN, H. G., STRIBECK, N., ASANO, T., 1991, *J. Polym. Sci.:B: Polym. Phys.*, **29**, 819.

SNEDDON, I. N., 1965, *Int. J. Engng. Sci.* **3**, 47.

SIMMONS, G., WANG, H., 1971, *Single Crystal Elastic Constants and Calculated Aggegate Properties: A Handbook 2nd. Ed.* (Cambridge, Massachusetts: The M. I. T. Press).

TABOR, D., 1951, *The Hardness of Metals* (New York: Oxford C. Press).

TURNBULL, A., WHITE, D., 1996, *J. Mat. Sci.* **31**, 4189.

VANCOILLE, E., CELIS, J. P., ROOS, J. R., 1993, *Thin Solid Films*, **224**, 168.

First set of experiments

P_{max} (mN)	$\dot{P}$ (mN/s)	Δt_{hold} (s)
147	13.2	6
147	13.2	11
147	13.2	20
147	13.2	40
147	13.2	200
147	13.2	600
147	13.2	1000

Second set of experiments

P_{max} (mN)	$\dot{P}$ (mN/s)	Δt_{hold} (s)	Δt_{hold} (s)
147	0.47	6	200
147	1.32	6	200
147	4.41	6	200
147	6.62	6	200
147	13.2	6	200

Third set of experiments

P_{max} (mN)	t_{load} (s)	Δt_{hold} (s)
0.98	7	6
1.96	14	6
4.90	10	6
9.8	7	6
147	11	6
245	10	6

TABLE 1

CAPTION TO TABLE

Table 1. Experimental parameters used in the three sets of experiments.

CAPTION TO FIGURES

Figure 1. Compliance curve for aged amorphous PET ($\dot{P}$ = 6.6 mN/s; Δt_{hold} = 200 s).

Figure 2. Double logarithmic plot of hardness versus holding time. ○: compliance method, cylindrical punch approximation, A=24.5 h_p^2; □: compliance method, cylindrical punch approximation, A=24.5 h_c^2; ●: compliance method, power law fitting method, A=24.5 h_c^2; ◊: imaging method.

Figure 3. Plot of hardness as a function of time during the loading cycle. ○: cylindrical punch approximation, A=24.5 h_p^2; □: cylindrical punch approximation, A=24.5 h_c^2; ●: power law fitting method, A=24.5 h_c^2.

Figure 4. a) Hardness variation with the maximum penetration depth of the indenter. Symbols as in figure 2. Question mark: limit in the imaging method resolution. b) Corrected hardness values as a function of the maximum penetration depth reached by the indenter. ○: cylindrical punch approximation, A=24.5 h'^2_p; ●: power law fitting method, A=24.5 h'^2_c.

Figure 5. Plot of Young's modulus values as a function of the holding time. Symbols as in figure 3.

Figure 6. Plot of $\Delta P/\Delta h$, as calculated using the cylindrical punch approximation, and $(\partial P/\partial h)_{max}$, as calculated using the power law fitting method, versus Δt_{hold}.

Figure 7. Load-displacement curves for different holding times.

Figure 8. Young's modulus versus loading time. Symbols as is figure 3. (a) Δt_{hold} = 6s; (b) Δt_{hold} = 200s.

Figure 9. Load-displacement curves for loading times of 11s (dashed line) and 311s (solid line): (a) Δt_{hold} = 6s; (b) Δt_{hold} = 200s.

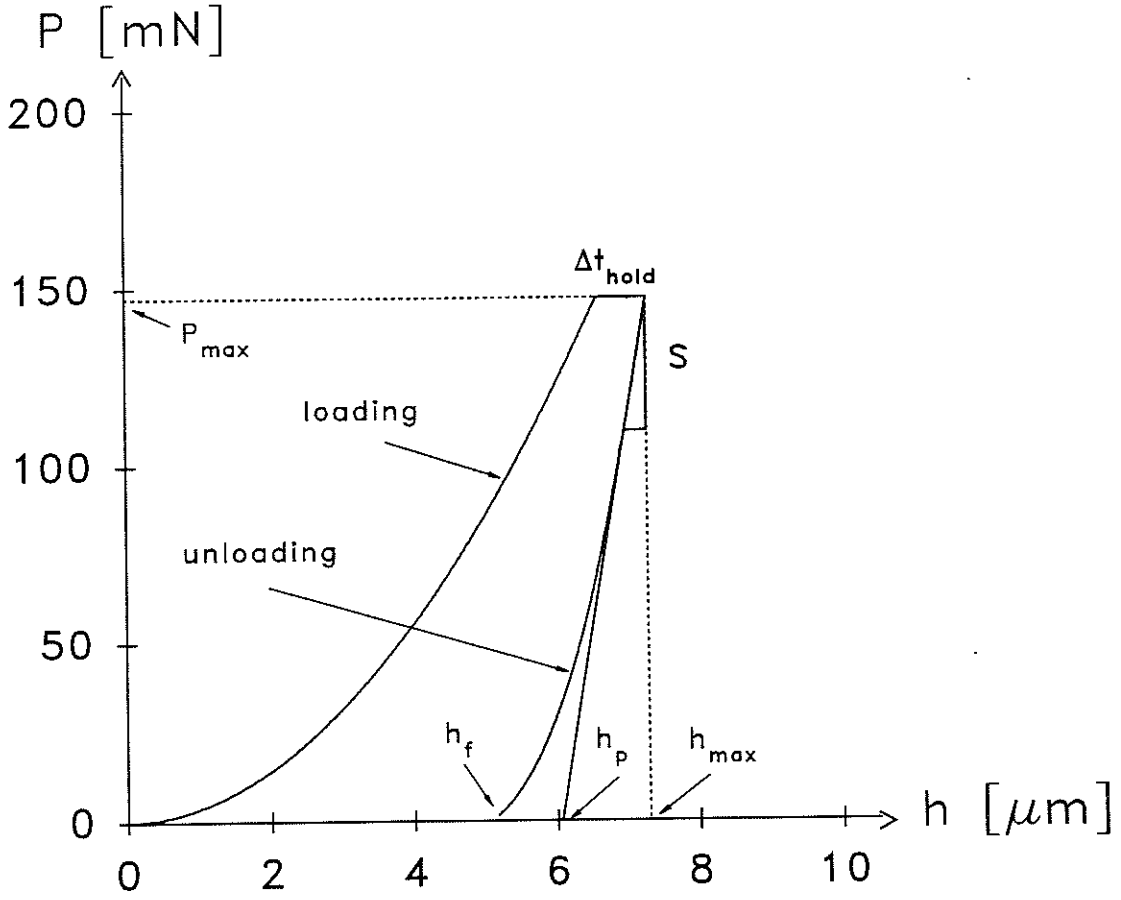
P [mN]
200
150
100
50
0
0
2
4
6
8
10
h [μm]
Δt hold
P max
S
loading
unloading
h f
h p
h max

Figure 1

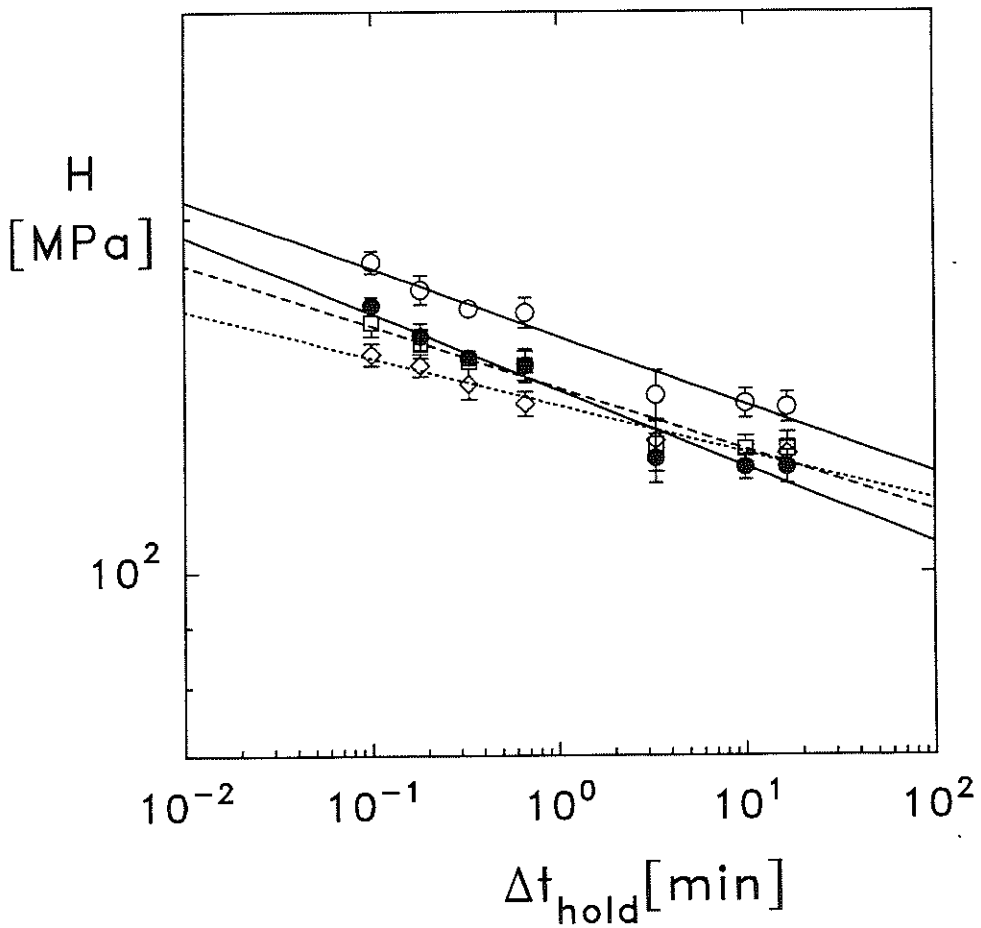

Figure 2

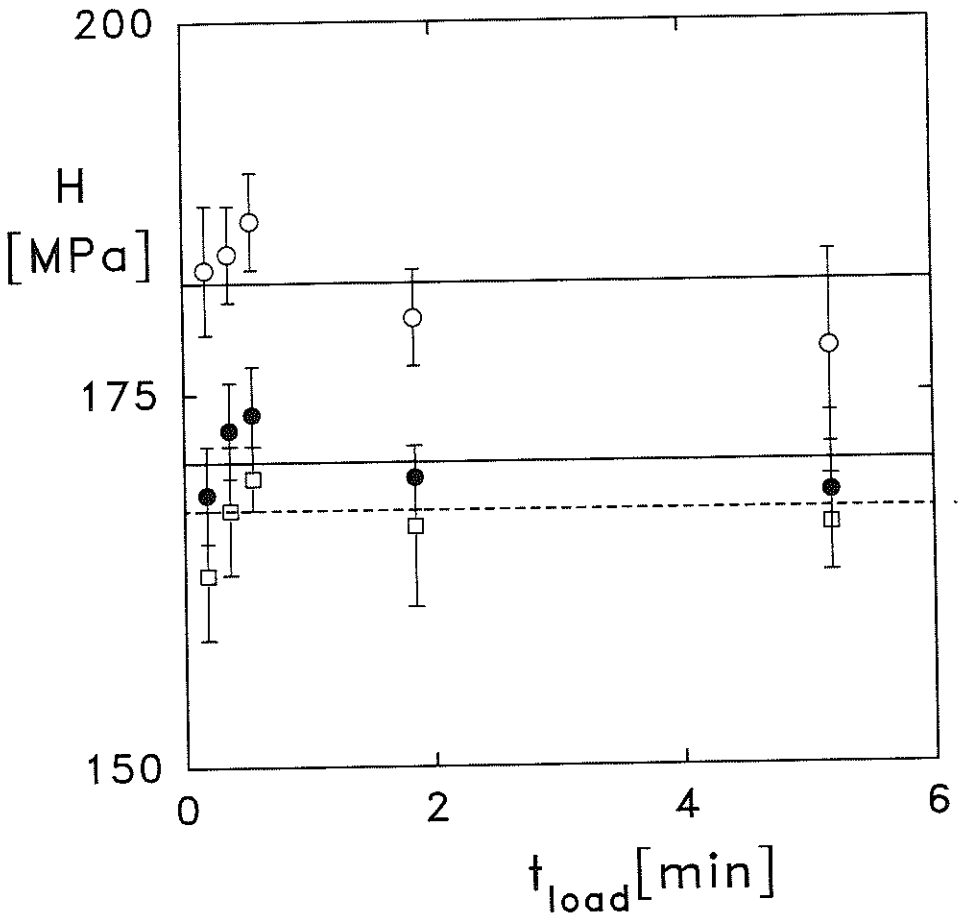

Figure 3

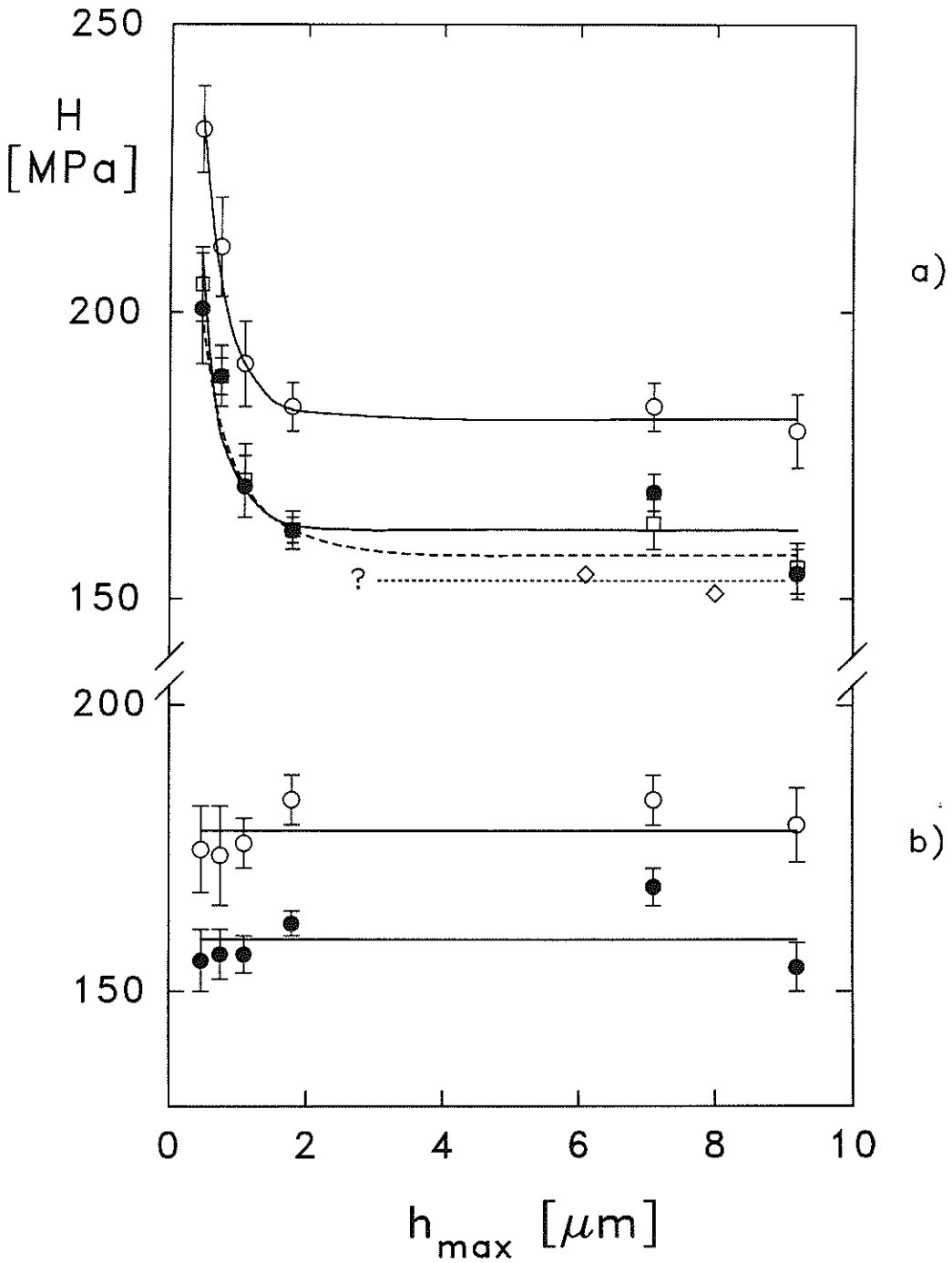

Figure 4

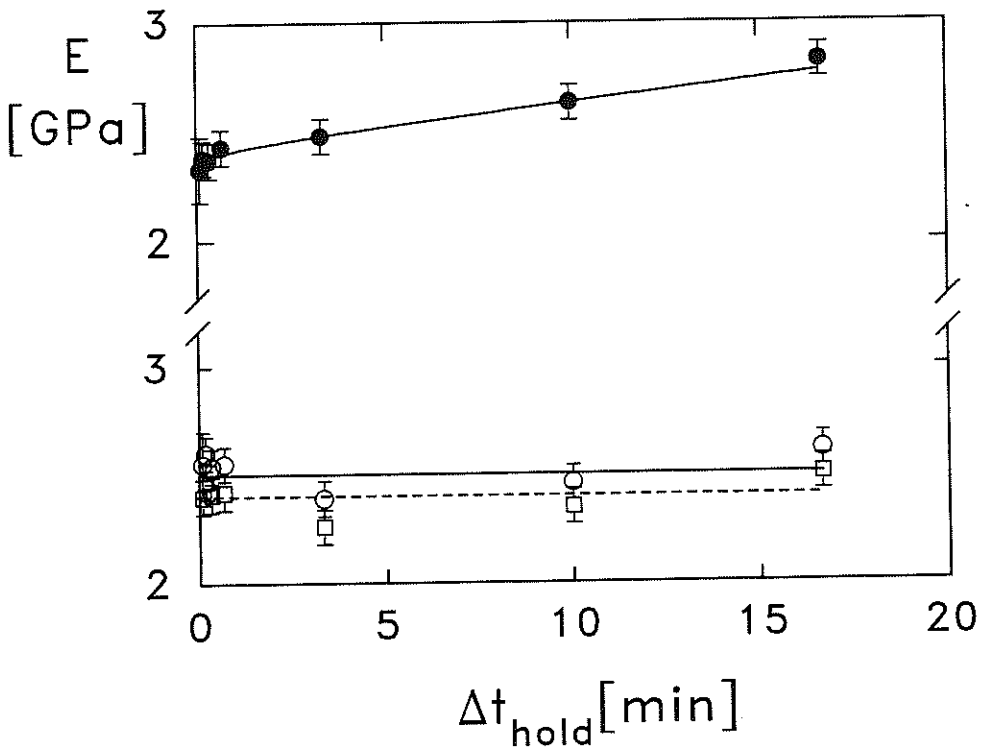

Figure 5

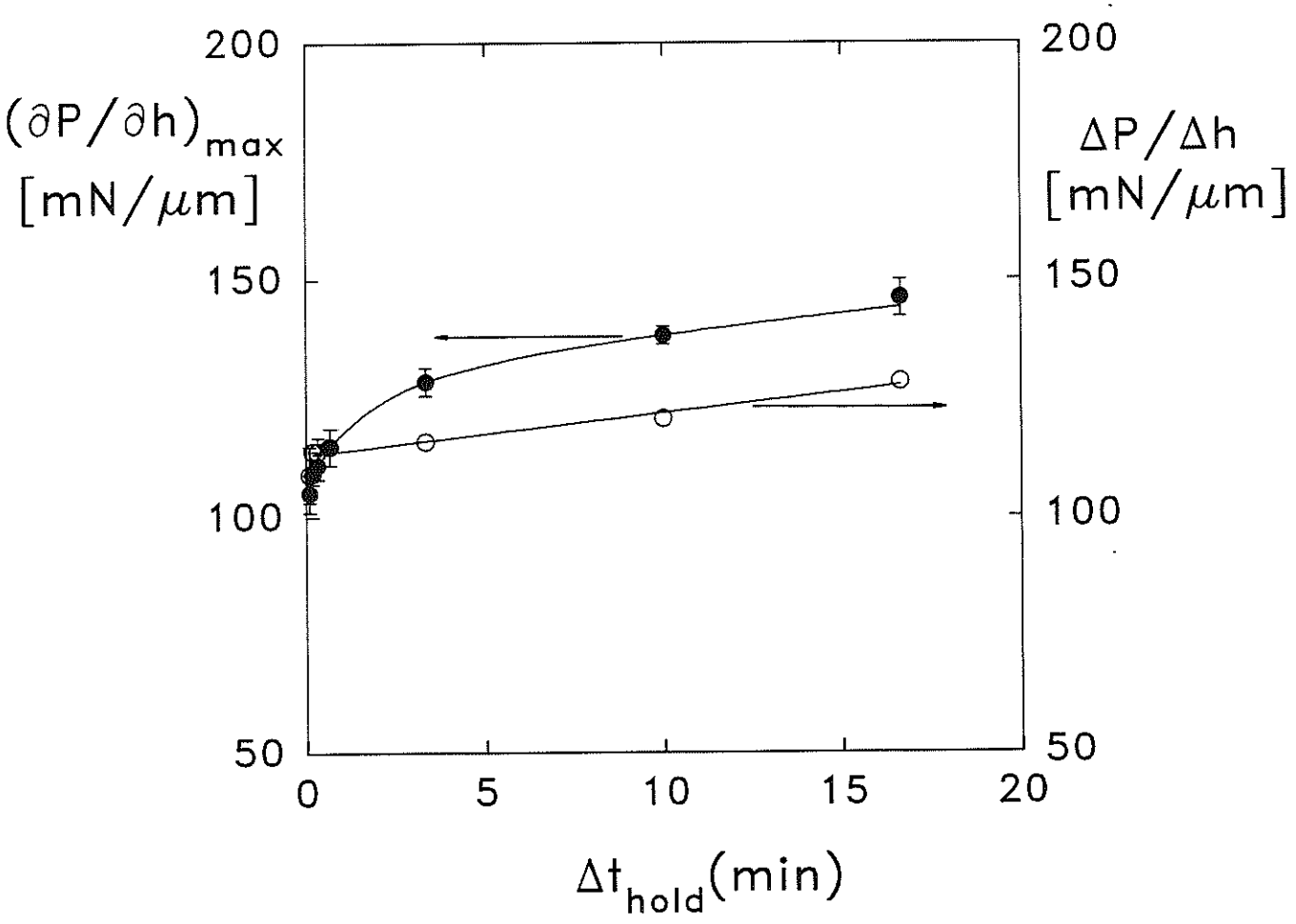
200
150
100
50
$(\partial P/\partial h)_{max}$
[mN/μm]
200
150
100
50
ΔP/Δh
[mN/μm]
0
5
10
15
20
Δt_{hold}(min)

Figur 6

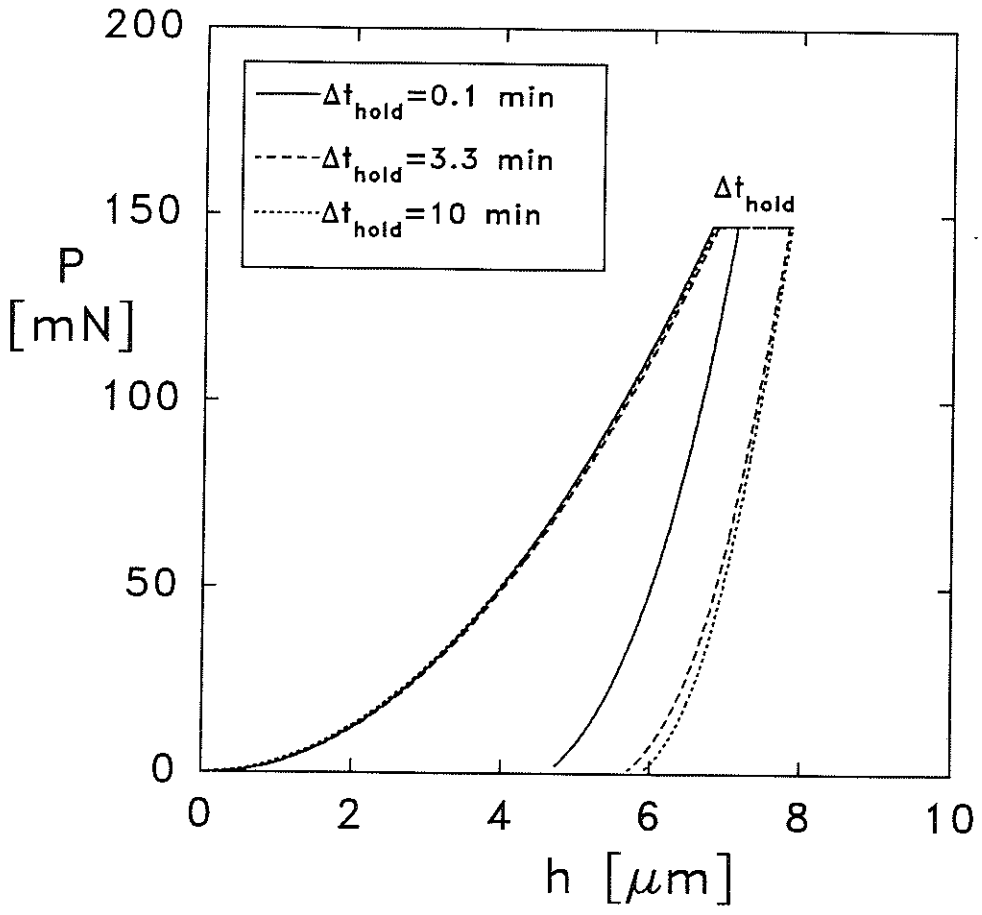
200
150
100
50
0
P
[mN]
0
2
4
6
8
10
h [μm]
Δt_hold=0.1 min
Δt_hold=3.3 min
Δt_hold=10 min
Δt_hold

Figure 7

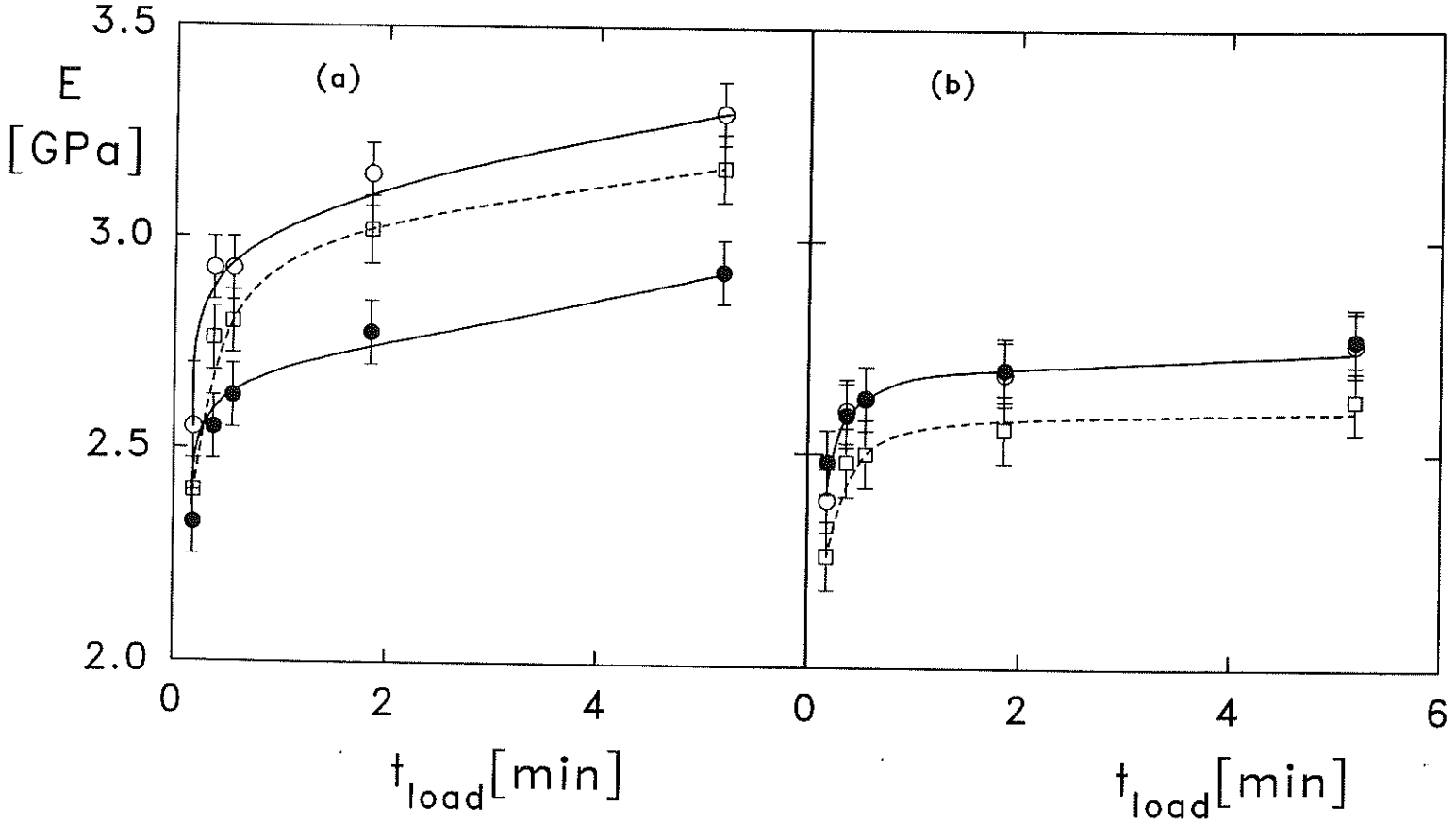

Figure 8

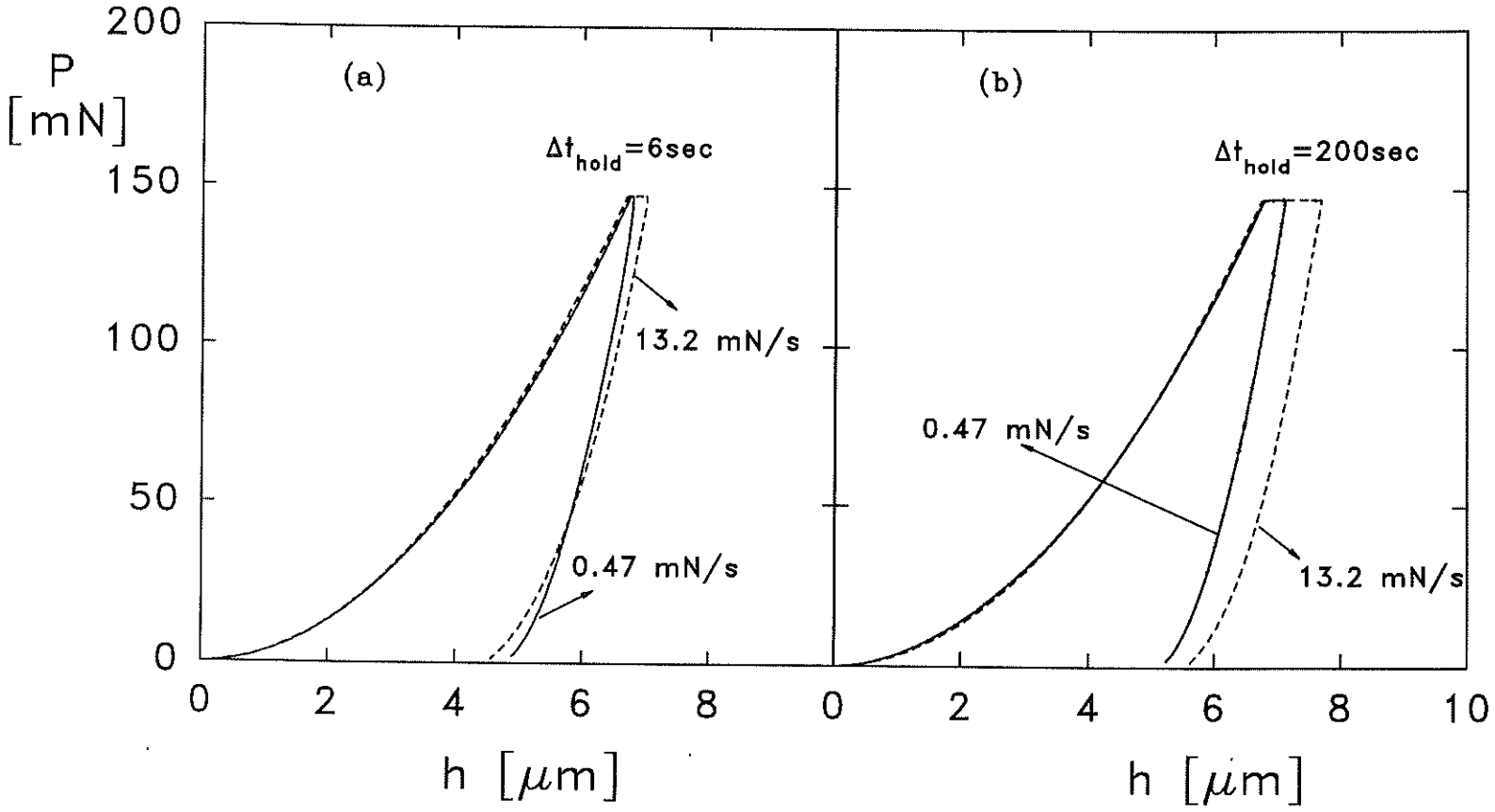
200
P
[mN]
150
100
50
0
(a)
Δt_{hold}=6sec
13.2 mN/s
0.47 mN/s
0
2
4
6
8
h [μm]
(b)
Δt_{hold}=200sec
0.47 mN/s
13.2 mN/s
0
2
4
6
8
10
h [μm]

Figure 9